

A multiband study of Hercules A. I. *ROSAT* observations of the intracluster medium

Nectaria A. B. Gizani^{1,2} and J. P. Leahy,²

¹ *Institute of Astronomy and Astrophysics, National Observatory of Athens, I. Metaxa & B. Pavlou, Lofos Koufou, Palaia Penteli, 15236 Athens, Greece.*

² *University of Manchester, Jodrell Bank Observatory, Macclesfield, Cheshire SK11 9DL, UK.*

6 July 2018

ABSTRACT

We have made *ROSAT* PSPC and HRI X-ray observations to study the intracluster gas surrounding the powerful radio source Hercules A. The cluster is luminous in X-rays ($L_{\text{bol}} = 4.8 \times 10^{37}$ W), although apparently poor in optical galaxies, and the host of the radio source is the central dominating galaxy of the cluster.

The azimuthally-averaged X-ray surface brightness profile is well fitted by a modified King (β) model, with core radius $r_c = 121 \pm 10$ kpc and $\beta = 0.74 \pm 0.03$, but the cluster is elongated parallel to the radio source, especially on the scale of the radio lobes, and fits to individual quadrants give a core radius 50 per cent larger along the radio axis. Part of this elongation appears to be associated with enhanced X-ray emission superimposed on the outer radio lobes, which extend to just over $2r_c$. There are no obvious depressions in the X-ray emission coincident with the radio lobes, as expected if the relativistic plasma displaces the ICM. However, we show that these depressions may be quite weak, essentially because the main part of the lobes are outside the cluster core. From the surface brightness profile for the PSPC data the X-ray emission extends out to ~ 2.2 Mpc radius.

In the absence of the powerful jets (which must be a transient phenomenon on cosmological timescales), we would expect a cooling flow at the centre of the cluster; but currently it must be substantially disturbed by the expansion of the radio lobes. The PSPC spectrum reveals a cool component of the ICM with $0.5 \lesssim kT \lesssim 1$ keV in addition to the ≈ 4 keV component detected by *ASCA* and *BeppoSAX*. The central cooling time could be as low as 2 Gyr if the cool component is centrally concentrated, otherwise it is around 6 Gyr. Cooling is significant on a Hubble time to a radius of about 90 kpc. The modelled central electron density of $n_0 = 1.0 \times 10^4 \text{ m}^{-3}$ is typical for modest cooling flows.

Finally, we have detected faint X-ray emission from a compact central source, with size < 15 kpc and luminosity $\approx 2 \times 10^{36}$ W.

Key words: galaxies: active - clusters: individual: Hercules A; X-rays: galaxies;

1 INTRODUCTION

Hercules A (3C 348) is the fourth brightest DRAGN¹ in the sky at low frequencies. At a low redshift of $z = 0.154$, its power at 178 MHz is $P_{178 \text{ MHz}} = 1.9 \times 10^{27} \text{ W Hz}^{-1} \text{ sr}^{-1}$, with $H_0 = 65 \text{ kms}^{-1} \text{ Mpc}^{-1}$ and $q_0 = 0$ (used throughout this paper).

Hercules A is identified with a very elongated cD galaxy (e.g. Sadun & Hayes 1993; Baum et al. 1996), with absolute magnitude -23.75 in the R-band (Owen & Laing 1989). It appears to lie at the center of a poor, faint cluster, although measurements of the cluster richness may be uncertain (Owen & Laing 1989; Yates, Miller & Peacock 1989; Barthel & Arnaud 1996).

Radio galaxies with the radio and optical luminosity of Her A nearly all show hotspot-dominated Fanaroff-Riley II structure (Ledlow & Owen 1996), but Her A is an exception (Dreher & Feigelson 1984). Its structure is dominated

¹ Double Radiosource Associated with Galactic Nucleus; see Leahy (1993) or Leahy, Bridle & Strom (<http://www.jb.man.ac.uk/atlas/>) for a full definition.

by its twin jets, which are quite different in appearance. The eastern one is the brightest (highest flux density) radio jet in the sky, and contributes a substantial fraction of the radio luminosity of Her A; a weaker jet to the west leads to a striking series of shells which dominate the western lobe. There are no compact hotspots. The structure is formally FR class I, but does not resemble typical FRI objects in detail.

X-ray emission from the Hercules A cluster was first detected by the *Einstein Observatory* (Feigelson & Berg 1983; Dreher & Feigelson 1984). They estimated the 0.2–4 keV luminosity as 2×10^{37} W. This is typical of a richness 0 to 1 Abell cluster (Abell 1958). In their deprojection analysis of the *Einstein* data on clusters of galaxies, White, Jones & Forman (1997) list Hercules A as a possible large cooling flow, although their best-fit model had a zero inflow rate due to their low spatial resolution.

Barthel & Arnaud (1996) have shown that Hercules A and other radio galaxies embedded in dense cluster gas are anomalously radio-loud (for their far-infrared luminosity), as expected because their confinement is more effective, reducing adiabatic expansion.

In this first paper of a series of three, we report observations of Hercules A in X-rays made with the *ROSAT* PSPC and HRI detectors. Gizani & Leahy (2002, hereafter Paper II) present new VLA observations of this powerful DRAGN, and we discuss the results derived from the spectral index and projected magnetic field/fractional polarization images all at $1''.4$ resolution. In Paper III (Gizani, Leahy & Garrington in preparation) we combine the results of Papers I and II to study the magnetic field of the cluster gas surrounding the DRAGN. Preliminary reports have already been published by Gizani & Leahy (1996, 1999). Our observations have also been discussed, in less detail, by Siebert, Kawai & Brinkmann (1999).

Sections 2 and 3 describe the observations and data reduction for the PSPC and HRI respectively. In Section 4 we analyse the radial surface brightness profile to infer the density distribution in the Her A cluster. In section 5 we compare the radio and X-ray structures to search for detailed correspondences, and review observations of related objects to put our results into context. Section 6 gives our conclusions.

2 PSPC OBSERVATIONS AND DATA REDUCTION

The total observing time with the PSPC detector was 8065 s, giving a live time of 7876 s. There were 5 observation intervals during 1993 August 19 – 31. These data were processed with the ASTERIX package, which is the U.K. X-ray data analysis package running within the Starlink ADAM/ICL environment.

The raw data, in MPE format, were pre-processed and converted to the ASTERIX internal format. Then they were ‘cleaned’ using standard housekeeping parameters (Osborne 1993): to ensure good aspect solutions, we only accepted times with $ASP_ERR \leq 1$, which removed 3 seconds of data. We have found no significant difference by applying screening to the spectral analysis for low particle background using

the master veto rate (EE-MV) < 170 . Therefore in the following analysis we have included all data.

2.1 Spectral Analysis

The X-ray emission from Her A is sufficiently compact that the radial variation in sensitivity in the *ROSAT* field can be neglected. We therefore extracted a background-subtracted spectrum in ASTERIX using the normal ‘point source’ procedure. We used a source region with radius 4.7 arcmin, and a background taken from an annulus extending to 9 arcmin. The background-subtracted spectrum was corrected for exposure, dead time, vignetting, and for photons scattered out of the detect cell (assuming a point source model).

The spectrum was processed with the FTOOLS program GRPPHA using the binning recommended by Briel et al. (1996). The data and response function were then read into XSPEC for spectral fitting.

We fitted a MEKAL model (Kaastra 1992) with neutral absorption using the XSPEC 11.0 cross-sections (Balucinska-Church & McCammon 1992), and Anders & Grevesse (1989) relative abundances. We do not consider $N_H < 5.5 \times 10^{20}$ cm $^{-2}$ as this is ruled out by HI absorption (Colgan, Salpeter & Terzian 1988), which detects only cold HI clouds and so is a lower limit. We use $N_H = 6.2 \times 10^{20}$ cm $^{-2}$ Stark et al. (1992) which is in excellent agreement with the best fit N_H for our X-ray spectrum. A single-temperature fit for $Z = 0.3$, a metallicity value typical of clusters, which is consistent with the data, gives $kT = 2.52^{+0.52}_{-0.36}$ keV, very similar to that found by Siebert et al. (1999). However, observations at higher energies give higher values for the best-fit temperatures: the LECS detector on *BeppoSAX* gives ≈ 3 keV in the 0.2–4 keV band, while the 1.5–9.5 keV MECS detector gives $kT = 4.8 \pm 0.6$ keV and $Z = 0.36 \pm 0.15$ (Trussoni et al. 2001). The 0.8–9 keV *ASCA* data of Siebert et al. are in excellent agreement with this, but Siebert et al. prefer a fit including a weak AGN component (consistent with the HRI image, see below), which gives $kT = 4.25^{+1.00}_{-0.66}$ keV and $Z = 0.44 \pm 0.13$. At this metallicity the PSPC best-fit temperature becomes $2.7^{+0.6}_{-0.4}$ keV, still not enough for reconciliation with *ASCA* & MECS. Thus, as noted by Siebert et al., the combined results suggest that there is a multiphase cluster gas around Hercules A, and none of the single-temperature fits can be taken at face value.

We have therefore tried a two-temperature fit to the PSPC spectrum with metallicity fixed at 0.44 and the hotter component fixed at 4.25 keV. For completeness we included a power-law component with $\Gamma = 1.9$ and normalization fixed to yield the point-source flux derived in our image analysis (see below), although this is too weak (about 5 per cent of the total counts) to significantly affect the fit. With one extra free parameter, the fit improves by $\Delta\chi^2 = 3.5$: the best fit temperature for the cool component is 0.71 keV, with a 1σ range 0.44–1.01 keV; Fig. 1 shows this model overlaid on the observed spectrum for Hercules A. Although such a two-component model must be over-simplified, the PSPC response varies little with temperature or metallicity for gas above 3.5 keV, so the components plausibly stand for a ~ 4 keV hot matrix, and a cooling-flow region, which can clearly comprise a range of temperatures given the uncertainty in the best-fit value. The cool gas could also be associated with

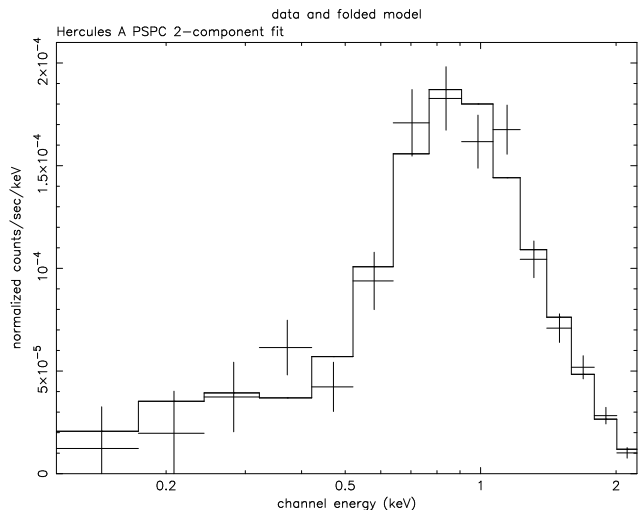


Figure 1. The background-subtracted PI spectrum of Hercules A with the absorbed 2-temperature MEKAL model fitted. Model parameters are $N_H = 6.2 \times 10^{20} \text{ cm}^{-2}$, $kT = 4.25$ and 0.69 keV , $Z = 0.44$ and $z = 0.154$, relative normalization 11.8:1 (corresponding to hard band flux ratio 6.0:1). Reduced $\chi^2=1.21$, with 12 degrees of freedom.

the radio lobes, as seen in *XMM* and *Chandra* observations of Vir A (Belsole et al. 2001), Hyd A (Nulsen et al. 2002), and Per A (Allen et al. 2001a), in each of which the radio jets seem to be dredging low-entropy gas out of the cluster centre. The excellent fits of single-temperature models to the MECS and *ASCA* spectra do suggest that there is little gas at intermediate temperatures. The cool component contributes 11–21 per cent to the *ROSAT* count rate (excluding the central compact source) with the higher contributions at the higher temperatures, and little dependence on metallicity. However, because it is dominated by line emission, its normalization in terms of emission measure depends strongly on metallicity.

The absorption-corrected bolometric luminosity of the Hercules A cluster is $L_{\text{bol}} \simeq 4.8 \times 10^{37} \text{ W}$ (see Section 4). The $kT - L_{\text{bol}}$ relation for cooling flow clusters of Allen & Fabian (1998) implies a temperature of around 3.6 keV for such a luminosity (with quite large uncertainty), consistent with the *ROSAT*, *BeppoSAX* and *ASCA* results.

Unfortunately in our PSPC data there are too few counts outside the central resolution element to allow meaningful determination of the spectrum as a function of radius, so we cannot investigate any radial temperature gradients. Radial spectral analyses of the *ASCA* and *BeppoSAX* data by Siebert et al. and Trussoni et al. were also inconclusive, unsurprisingly in view of the lower resolution of these instruments. We show below that the cool gas could represent the majority of the emission from the core of the cluster, but the phases could also be mixed, perhaps as a result of the expansion of the radio lobes.

We derive the gas density from radial profile fits to our X-ray images. Following Leahy & Gizani (2001) we evaluated the conversion factor between brightness and emission measure, for our assumed ‘hot’ component: for S in ct s^{-1} in the PSPC hard band (PI channels 52–201):

$$f_C(T, Z, z) = 2.05 \times 10^{-24} \text{ m}^5 \text{ ct s}^{-1} \text{ sr}^{-1},$$

The conversion factor between ct s^{-1} and W m^{-2} (0.1–2.4 keV, absorbed) is $f_E/f_C = 1.55 \times 10^{-14} \text{ W m}^{-2} / \text{ct s}^{-1}$, and the cooling function, giving the conversion factor for ‘bolometric’ (0.01–100 keV) emissivity is:

$$\Lambda(T, Z) = 1.90 \times 10^{-36} \text{ W m}^3.$$

Our model gives

$$I / (\text{ct s}^{-1} \text{ sr}^{-1}) = 6.31 \times 10^{-5} EM / (\text{m}^{-6} \text{ kpc}), \quad (1)$$

where $EM = \int n_e n_H dl$ is the emission measure. For metallicities in the observed range for clusters, $0.16 < Z < 0.5$ (e.g. Scharf & Mushotzky 1997), $f_C(T, Z)$ varies by less than 10 per cent from our quoted value for $2.4 < kT < 10 \text{ keV}$. However $f(T, Z)$ for the cool component increases rapidly with metallicity; for $Z = 0.5$ it reaches twice our quoted value for $0.5 < kT < 1 \text{ keV}$. If the cool gas is concentrated in the cluster core it likely has higher-than-average metallicity and densities will be *over*-estimated in that region by up to 50 per cent, but nearly correct at larger radii; if it is distributed throughout the cluster with a similar metallicity to the hot gas, the average density will be over-estimated by a few percent.

2.2 The PSPC Image

Fig. 1 shows that, due to Galactic neutral hydrogen absorption, there are few source photons in the channels below 0.5 keV; on the other hand the background is highest in these channels. Therefore the signal-to-noise ratio (SNR) is much higher in the hard band, and therefore we confine image analysis to this band. This has the added benefit that the PSF is smallest in this band and varies relatively little with energy. We created a background subtracted hard-band image using the same region as for the spectral analysis, and corrected for exposure, dead time, and vignetting. The position scale was set by aligning the X-ray peak with the radio core. The offset of about 6 arcsec is consistent with the known pointing errors of *ROSAT*.

The resulting image, smoothed with a gaussian of FWHM 20 arcsec, is presented in Fig. 2. Note that the fractional uncertainty in brightness in a photon image smoothed with a gaussian is $\sqrt{1/2N}$ (Hardcastle, Worrall & Birkinshaw 1998), where N is the number of photons within the smoothing effective area (hereafter ‘beam’) $A = 1.13(\text{FWHM})^2$. In Fig. 2, $N \approx 0.9$ for the background, so the errors for faint emission are highly non-gaussian.

2.3 The Radial Brightness Profile

The faint outer halo of the Hercules A cluster is best seen in the radial brightness profile; however in this case the background is detected with good signal-to-noise and it was necessary to take more care over background subtraction before we could obtain an accurate profile. In order to allow the background to be fitted as part of the overall profile fitting, our procedure was as follows.

We located the clearly-detected point sources in the 40-arcmin diameter central portion of the PSPC field, using a simple peak finder applied to the image in Fig. 2. Peaks

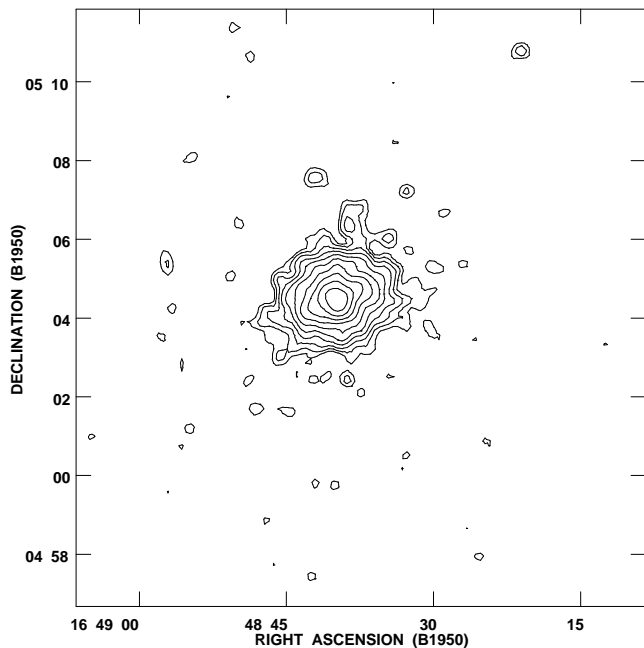


Figure 2. The PSPC image of Hercules A. The image has been smoothed with a 20-arcsec FWHM gaussian. Resolution is 32 arcsec FWHM, including the instrumental PSF. The image was projected into B1950.0 coordinates in AIPS. The first contour is at $5.29 \times 10^{-10} \text{ W m}^{-2} \text{ sr}^{-1}$, and contours are separated by ratios of $\sqrt{2}$. The background is $\approx 1.6 \times 10^{-10} \text{ W m}^{-2} \text{ sr}^{-1} \equiv 0.9 \text{ ct beam}^{-1}$.

within 5 arcmin of the cluster centre were not included in the list as they are likely to be substructure or random fluctuations in the cluster gas (the only clear point source in this region in our HRI image is not detected by the PSPC). We created a mask consisting of discs with radii ranging from 25 to 90 arcsec (depending on distance from the field centre, to allow for aberration) centred on each source. This was applied to the raw data, and a radial profile extending out to $0^\circ.3$ was extracted, by integrating in rings around the cluster centroid using IRADIAL, with a radial bin size of 2.5 arcsec.

The raw data must be corrected for vignetting, exposure and dead time. The correction as a function of radius is not explicitly available from ASTERIX, so we derived it by taking the ratio of profiles derived from the corrected image (from XRTCORR) and the image from XRTSUB. To model the vignetting of the background, we also made a profile of the ‘background’ image created by XRTSUB. (The same mask was applied in all cases). The model background includes a small (1.3 per cent) unvignetted contribution from the particle background, but this negligible in our case. The model was derived from a ‘spectral image’ of the background annulus, in which the band was divided into 5 channels to accurately account for the energy-dependent radial vignetting. Since this region contains some source emission, we regarded the amplitude of the background as a free parameter in our fitting procedure (Section 4). All profiles were converted to ascii files using AST2TXT, and further processed with our own software.

The correction was applied to the raw data, to the associated errors (initially assumed equal to poisson errors),

and to the background model. Photons from an on-axis point source will not be affected by vignetting, so to compensate for the application of the correction to all the photons, we also applied a correction (normalized to unity at the centre) to our PSF model.

There is a slope in the background across the PSPC field of view, with an amplitude of $\sim \pm 15$ per cent at 15 arcmin from the centre; however this is cancelled by azimuthal averaging. To get an idea of smaller scale fluctuations that might affect our profile, we summed the masked and corrected image between $0^\circ.15$ and $0^\circ.3$ in six radial bins; the rms between bins was 4 per cent of the (unsubtracted) background, consistent with expected poisson fluctuations. We note that each radial bin has a similar solid angle to the sky region occupied by the cluster. Since it would be fortunate if the large-scale structure in the background were purely a linear slope, we conservatively assume there may be systematic fluctuations in the azimuthally-averaged background at the 3 per cent level.

The profile was binned to give binwidths ≥ 5 arcsec, and a signal-to-noise ratio (SNR) of $>5:1$, subject to a maximum bin width of 90 arcsec. The SNR was calculated after background subtraction, and the error used included our 3 per cent systematic uncertainty, added in quadrature to the poisson uncertainties. All bins contained > 25 photons before background subtraction.

The binning and fitting procedure (Section 4) was iterated a couple of times to ensure self-consistency. The final result is shown as the starred points in Fig. 4.

3 HRI DATA ANALYSIS

Our HRI observation was split into two periods separated by six months. The first, with a duration of only 1232 s, was on 1996 February 18. The second, with the remaining 21516 s, contained 12 observational intervals during 1996 August 27–30. Observations taken six months apart have opposing spacecraft orientations and frequently show large pointing offsets (D. Harris, priv. comm.). Since there were no strong sources in the field to allow accurate alignment, we decided to analyse only the second dataset. We first corrected it for the timing error in the standard analysis which affected the aspect solutions (using a script distributed by the Harvard-Smithsonian Centre for Astrophysics). The data was processed in ASTERIX and FTOOLS.

Because of the uncertainty in spectral response of the HRI (e.g. Greiner et al. 1999), we did not attempt a spectral analysis. However, we did analyse the pulse-height analyser (PHA) distribution of source and background to try to optimise the signal-to-noise ratio (SNR). The background was determined in the annulus between 4 and 7 arcmin around Her A, which does not contain any background sources. The high HRI background makes it much less sensitive than the PSPC to very faint emission, so we decided to optimise the HRI image for the moderately bright emission around the radio lobes (at radii 50–100 arcsec), giving channels 3–7 as the best choice. These channels contain 83.3 per cent of the counts in a background-subtracted PHA spectrum of the source.

We made an image with the full spatial resolution (0.5-arcsec pixels) using channels 3–7, subtracted the background

(0.00464 ct pixel⁻¹, derived from the profile fitting in Section 4), and converted to count rate by dividing by the exposure time. No vignetting corrections were applied but these are unimportant within 5 arcmin (the background is dominated by charged particles which suffer no vignetting). We also did not correct for detector quantum efficiency variations, as these are not well determined at high resolution; we include a 4 per cent systematic error in the background to allow for this (c.f. Leahy & Gizani 2001).

We converted from observed count rate to emission measure in the same way as for the PSPC data, except that we used the observed PHA spectrum to estimate the fraction of the HRI counts that fall into our selected range of PHA channels. For our best fit model and our chosen PHA bands, the HRI is 2.86 times less sensitive than the PSPC, and this ratio varied by less than 2 per cent for any of the plausible models we tried. The lower sensitivity of the HRI is cancelled by the longer exposure time, so that the two images have nearly the same sensitivity to bright emission.

Fig. 3 shows a greyscale of our $\lambda 20$ -cm radio image (from Paper II) with contours from the HRI, with 10-arcsec smoothing, superimposed. Positions were again set by aligning with the radio; the HRI peak (after smoothing) was within 2 arcsec of the radio core. The HRI peak is not completely symmetric, but we suspect that this is due to aspect errors during the observation.

The radial profile for the HRI data was created using IRING in AIPS as there were no spatially-varying corrections to be applied. The raw bin size was 1 arcsec and the profile extended to 250 arcsec. Full details of the procedure are described by Leahy & Gizani (2001). The profile was binned in the same way as for the PSPC, except that we assumed a 4 per cent systematic error in the background and used minimum and maximum bin widths of 2 and 50 arcsec respectively. The background-subtracted profile is plotted in Fig. 4, multiplied by 2.86 to put it on the same scale as the PSPC data.

There are superficial differences between the PSPC image and the HRI image convolved to the same resolution, but these are approximately consistent with random noise: the apparent extension of the cluster peak emission, more or less perpendicular to the radio axis (see Fig. 2) is not confirmed by the HRI data. Whereas the PSPC seems to find a deficit of flux at $r \approx 100$ arcsec relative to a β model (see below), the HRI image shows a (marginally significant) plateau at about this radius, especially to the south-east, and in the ‘spur’ extending to the north of the cluster, (which is considerably more diffuse in the smoothed HRI image than in Fig. 2).

To get a best-possible image of the cluster on arcminute scales, we made a weighted average of the PSPC and HRI images. The PSPC data were smoothed with a 20 arcsec gaussian as before, while the HRI image was smoothed with a 31.5 arcsec gaussian to give approximately the same resolution, allowing for the ≈ 25 arcsec FWHM intrinsic PSF of the PSPC. Both images were converted to instrument-independent brightness units. Weighting was by the inverse $\sqrt{N/2}$ variance in the smoothed images, except that we did not let N fall below the average background value. The larger smoothing of the HRI data makes the latter about twice as sensitive in the cluster core, while at larger radii the lower background of the PSPC means that the latter

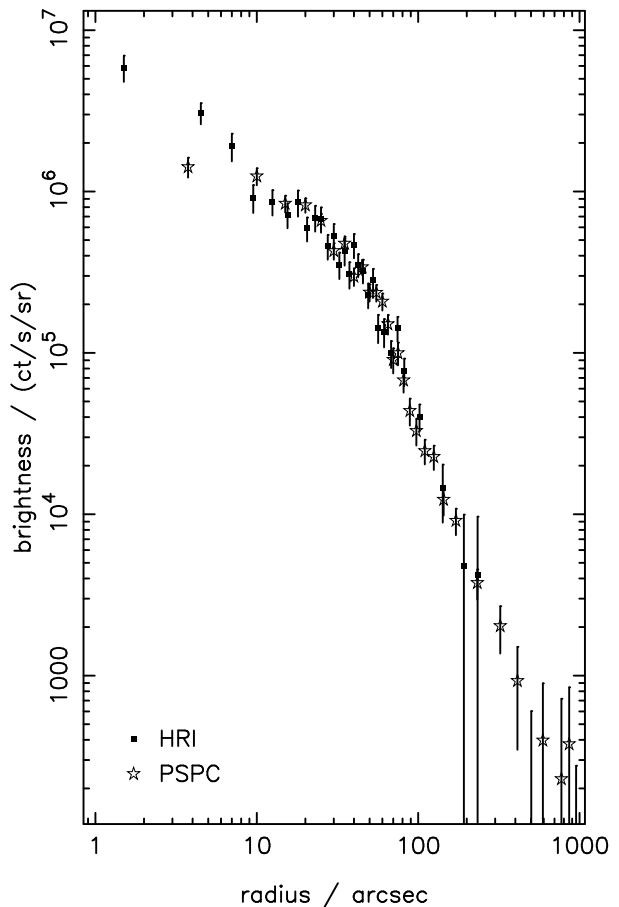


Figure 4. The X-ray surface brightness profile of the Hercules A cluster from *ROSAT* PSPC (stars) and HRI (squares), after backgrounds have been subtracted. Error bars are 1σ allowing for 4 per cent and 3 per cent uncertainty in the HRI and PSPC backgrounds respectively.

dominates. Fig. 5 shows contours of this weighted image superposed on the same radio image as in Fig. 3, this time displayed with a logarithmic transfer function to emphasise the faint emission projected across the cluster core.

The total radio emission extent is ≈ 540 kpc, comparable to the size of the X-ray gas visible in the images, but the radial profile in Fig. 4 shows that faint X-ray emission extends out to at least 2.2 Mpc radius.

4 MODEL FITTING OF THE SURFACE BRIGHTNESS PROFILE

Allowing for their different resolutions, the HRI and PSPC profiles are in good agreement. The profiles differ within ~ 20 arcsec of the centre due to the lower resolution of the PSPC, and are limited at large radii by the uncertainties in background level discussed in Sections 2.2 & 3.

We tried fitting the surface brightness profiles with various models, to find the electron density distribution in the Hercules A cluster. Among these were a King or β -model (King 1962; Cavaliere & Fusco-Femiano 1978), a de Vaucouleurs $r^{1/4}$ model and a combination (sum) of both. We confidently excluded the flat-topped ‘King-law’ profile,

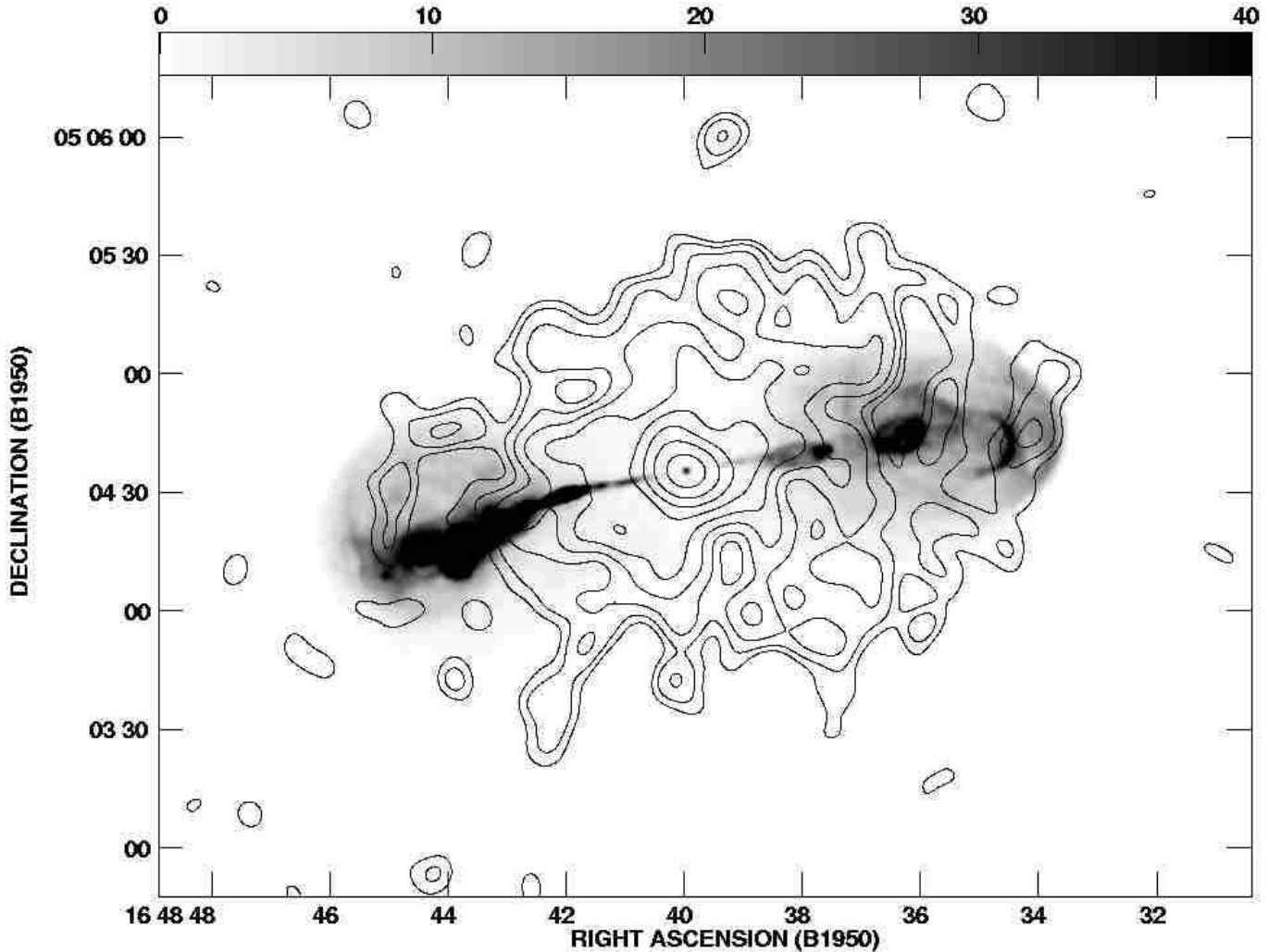


Figure 3. A grey-scale image of the Hercules A radio emission at 1.5 GHz with contours of the HRI X-ray image superimposed. The radio image has resolution 1.4 arcsec FWHM, and the greyscale range is 0 to 40 mJy beam⁻¹. The HRI image has been smoothed with a gaussian of FWHM 10 arcsec, giving an effective resolution of 11.5 arcsec including the instrumental PSF. Contours are separated by factors of $\sqrt{2}$ starting at 2.37×10^{-9} W m⁻² sr⁻¹ = 3.07 ct beam⁻¹ (3σ above the background). The background level (which has been subtracted) is 1.63×10^{-9} W m⁻² sr⁻¹ = 2.10 ct beam⁻¹.

as it failed to describe the brightness spike in the center of the cluster. The de Vaucouleurs model, as well as the model resulting from the sum of the latter with the King model, also failed, this time at larger radii. A somewhat better fit was obtained with an analytic ‘cooling flow’ model (Bertschinger & Meiksin 1986), but this still failed to represent the central peak. We therefore concluded that this peak was a discrete feature and not just part of a continuous brightness distribution.

We obtained a good fit from a combination of a β -model with a central point source. We emphasise that, although the β -model was originally proposed as an approximation to the isothermal sphere, it provides an accurate empirical fit to the emissivity in many ‘cooling flow’ clusters (White et al. 1997). For the point source we used the theoretical HRI PSF (David et al. 1998), as none of the background sources are bright enough to give a measure of the PSF width. This does not give a perfect fit to the centre of the radial profile, not surprisingly, in view of the obvious elongation of the peak in the image. Following Leahy & Gizani (2001), we also tried

fitting with a ‘blurred’ PSF to allow for aspect errors, but the improvement in the fit was only just significant at the 5 per cent level, when fitting the HRI data alone; for the better-constrained joint fit to HRI and PSPC, the improvement was insignificant. Hence we use the nominal PSF in the following. The construction of the HRI PSF followed the method of Leahy & Gizani (2001), which allows for the finite pixel size of the original image. For the PSPC, where accuracy is less critical because the compact component is only weakly detected, we simply evaluated the PSF model of Hasinger et al. (1995) at the centre of each 2.5-arcsec radial bin (assuming a photon energy of 1 keV). The results are given in Table 1. Since the PSPC background model has a slight radial dependence, in Table 1 we quote the value at the field centre. S is the point source flux and I_0 the central brightness of the β -model.

The PSPC profile fit was broadly consistent with that for the HRI, although the central peak is not clearly detected because the contrast against the cluster emission is much less with the lower resolution. To get a best estimate

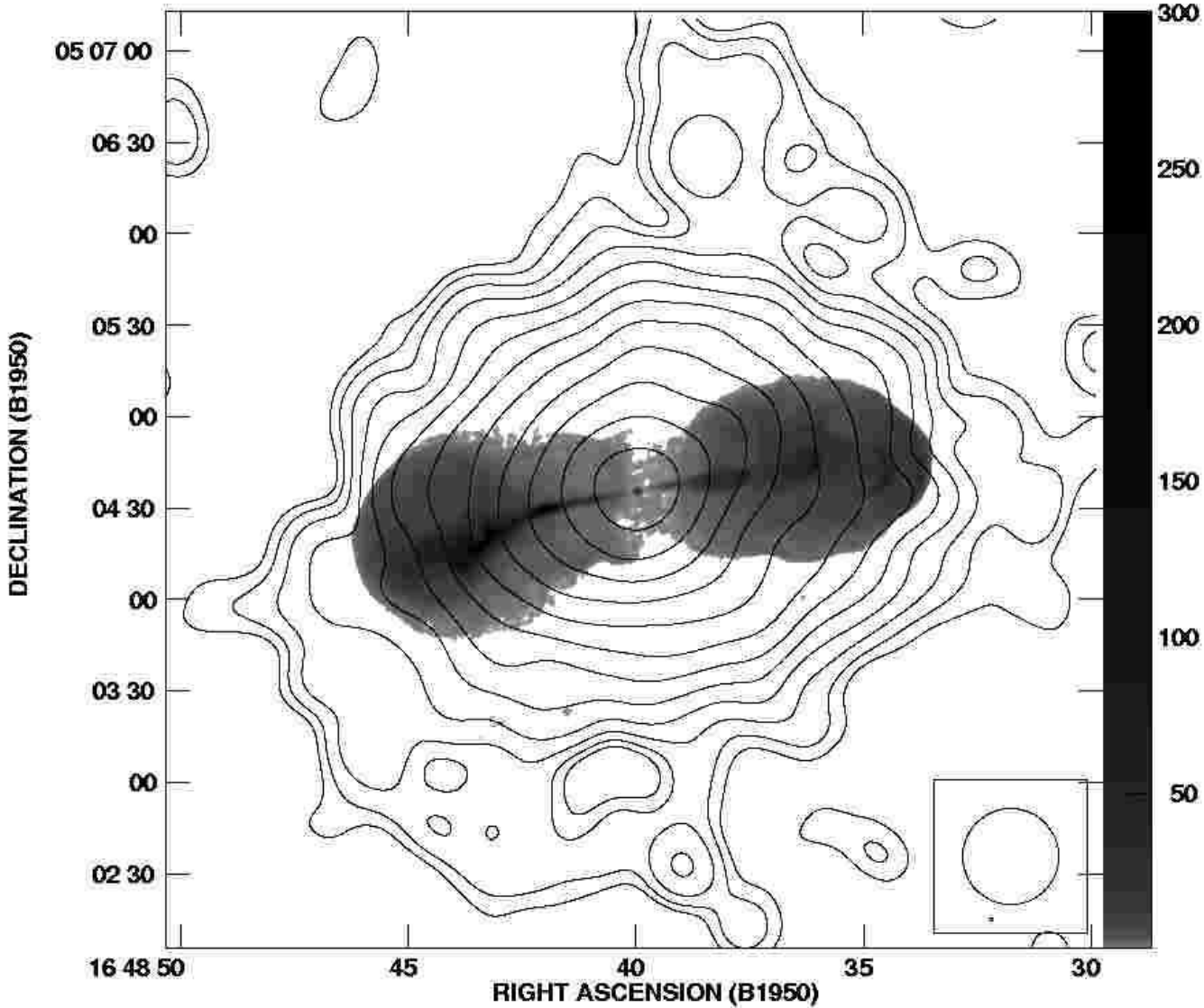


Figure 5. A contour map of the summed *ROSAT* PSPC and HRI image of the Hercules A cluster in the 0.5-2 keV band, overlaid on a grey scale of the 20 cm radio map. The radio image is displayed with a logarithmic transfer function, between 0.3 and 300 mJy. Contours are separated by a ratio of $\sqrt{2}$. The resolution of the X-ray contour map is $32''$, and of the radio image, $1''.4$. The first contour is at $2.94 \times 10^{-10} \text{ W m}^{-2} \text{ sr}^{-1}$, and contours are separated by a ratio of $\sqrt{2}$. The zero level has been subtracted. The boxed circle gives the smoothing beam of the HRI data, essentially the resolution of the X-ray map.

Table 1. The final results from the model fit to the surface brightness profiles

	S ct s ⁻¹	I_0 ct s ⁻¹ sr ⁻¹	r_c kpc	β	χ^2	Background ct s ⁻¹ sr ⁻¹
HRI only	0.0095 ± 0.0018	$9.6 \pm 0.9 \times 10^5$	117 ± 19	0.71 ± 0.08	25.5 (25 df)	1.05×10^5
PSPC only	0.0058 ± 0.0048	$10.7 \pm 1.6 \times 10^5$	112 ± 15	0.72 ± 0.04	39.5 (27 df)	9.59×10^3
Combined fit	0.0092 ± 0.0014	$9.6 \pm 0.6 \times 10^5$	121 ± 10	0.74 ± 0.03	65.8 (56 df)	9.60×10^3

HRI fluxes have been converted to the PSPC scale by multiplying by 2.86.

of the cluster structure, we fitted both profiles simultaneously, allowing the PSPC background to vary and keeping the HRI background fixed. The combined best fit is given in Table 1. We use the parameters found from this in our further analysis. The best fit is shown plotted against the data from each instrument in Fig. 6.

The combined fit is excellent for the HRI data. The HRI data contribute 25.6 to χ^2 of the combined fit, with 29 bins. The fit to the PSPC data is less good, $\chi^2 = 40.2$ with 32 bins. Within a radius of 100 arcsec, the HRI data is as sensitive as the PSPC, and the good fit to the former suggests that the poor PSPC fit is just a random error. The

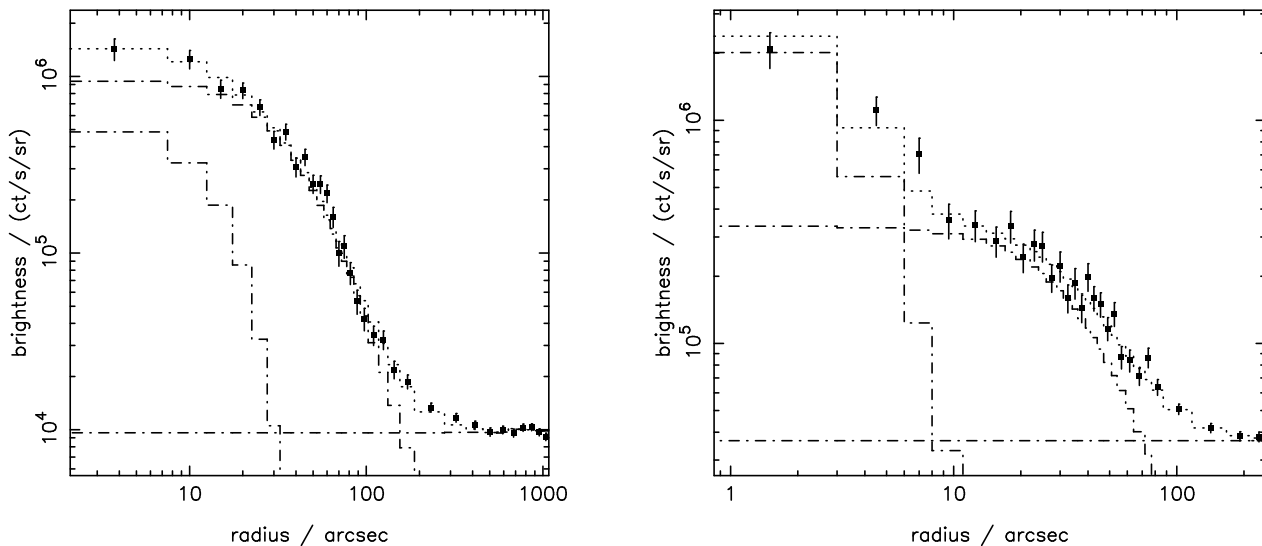


Figure 6. The best fit compact source + β model fit to the radial surface-brightness profiles of the Hercules A cluster. In each plot the combined model is given by the dashed line and the three components of the model (PSF, β model, and background) are given by dash-dot lines. (a) PSPC data. (b) HRI data.

PSPC does reveal excess emission compared to the β model at 200–400 arcsec.

The value found for β is within the range 0.5 to 0.8 found for most clusters (Jones & Forman 1984; Cirimele, Nesci & Trèvese 1997). Siebert et al. (1999) find $\beta = 0.63$ and a core radius of 90 kpc (for our H_0), but this is based on fitting the HRI data only, and only in a sector away from the radio lobes. We replicate their result in Section 5.1. The PSPC gives a much stronger constraint on β , and at radii much larger than the radio lobes and likely unaffected by them, so it makes sense to average all azimuthal angles.

To estimate the possible variability of the central source, we fitted the HRI and PSPC data separately, fixing the parameters of the β model and backgrounds to those found in the joint fit. The result is not well constrained because the core is so weakly-detected by the PSPC; we find an insignificant increase of 13 ± 36 per cent between the PSPC and HRI observations. As expected from the small contribution of the core to the total flux, any power-law spectral component was undetected in the *ASCA* and *Bep-poSAX* spectra (Siebert et al., Trussoni et al.); as Trussoni et al. point out, this does confirm that the core is not heavily obscured.

The integrated flux in the PSPC profile within 500 arcsec is 0.207 ± 0.005 ct s $^{-1}$, which slightly exceeds the combined flux in the model, due to the deviations from the model noted above. To get our best estimate for the total flux of the cluster, we subtract the central source, apply a 3 per cent correction to infinite radius (found analytically from our β model fit), and an 11 per cent correction to the total band (found by integrating the observed spectrum), PI channels 11–223, giving 0.227 ± 0.006 ct s $^{-1}$, corresponding to a 0.1–2.4 keV (absorbed) flux density of 3.04×10^{-15} W m $^{-2}$, a (rest frame, unabsorbed) luminosity of 3.00×10^{37} W, and a bolometric luminosity of 4.84×10^{37} W (all calculated for our two-temperature spectral model). These figures are

consistent with (but slightly lower than) the values derived from the much shorter RASS observation by Ebeling et al. (1998); they are in excellent agreement with the results from the long *Einstein Observatory* exposure analysed by White et al. (1997) (allowing for the different H_0, q_0 assumed in these studies).

We saw above that relatively cool gas contributes $f_{\text{cool}} \approx 15$ per cent of the cluster emission. This must have a density $\gtrsim 4$ times higher than adjacent hot gas for pressure balance, and is also likely a more efficient emitter (i.e. higher $f(T, Z, z)$). Thus *if* it is radially segregated (as in cooling-flow clusters), *then* it must nearly fill the cluster core; otherwise we would expect a two-scale core in emission (the central source cannot be the cooling-flow core, as its flux is less than half that of the cool component). In fact 11–21 per cent of the cluster emission comes from within 0.65–0.89 core radii for $\beta = 0.74$. Thus complete radial segregation is barely consistent, even if f_{cool} is at the upper end of the range (which we recall implies $\langle kT \rangle$ closer to 1 than 0.5 keV).

We have found the electron density from the emission measure, *EM*, and the conversion factor derived in Section 2.1 (recall this assumes $kT = 4.25$ keV). The electron density n_e of the β model cluster can be written as

$$n_e = \frac{n_0}{(1 + (r/r_c)^2)^{3\beta/2}} \quad (2)$$

Taking $n_e = 1.2n_H$, we find a central electron density $n_0 = 1.0 \times 10^4$ m $^{-3}$, suggesting a quite dense cluster, as typical cluster central number densities are of order 10^3 m $^{-3}$ (Jones & Forman 1984). If we have a cooling flow, the central density is probably overestimated by 30–50 per cent, as noted earlier; but the densities derived from our model (with n_0 as quoted) should be correct at $r > r_c$, since the model correctly predicts the brightness at all radii, and the cool component makes at most a small contribution at large r .

Table 2. The results from the 3-component model fit to the on-lobe profiles

	r_c kpc	β	χ^2
HRI only	149 ± 19	0.85 ± 0.11	28.5 (18 df)
PSPC only	148 ± 11	0.84 ± 0.05	23.3 (21 df)

Table 3. The results from the 3-component model fit to the off-lobe profiles

	r_c kpc	β	χ^2
HRI only	98 ± 13	0.65 ± 0.06	13.9 (13 df)
PSPC only	126 ± 11	0.83 ± 0.06	39 (18 df)

5 DISCUSSION

5.1 Interaction of the radio lobes with the cluster gas

We have looked for distortions in the cluster gas near the radio lobes, which might reveal interactions between the gas and the supposedly expanding lobes. As a first step we made radial profiles from the PSPC and the HRI data in four azimuthal sectors centered on the X-ray compact source. Two sectors were taken with position angles on the radio lobes (‘on-lobe’ profile), with a full width of 90° each, at PA 98° and -82° . The other two sectors had position angles off the lobes (‘off-lobe’ profile), with the remaining position angles. Tables 2 and 3 show the results of the best compact source plus β model fit to the on-lobe and off-lobe profiles. The free parameters were β and the core radius r_c ; the X-ray flux from the compact source, the central brightness, and the background were kept fixed to the values found from the combined fit in Table 1.

Figs. 7 and 8 show the on- and off-lobe profiles for the PSPC and HRI respectively. In each of the plots the combined model is given by dashed line and the three components (PSF, β model, and background) are given by dash-dot lines.

Table 2, from the profiles on the radio lobes, shows that PSPC and HRI agree well, and show that the core of the gas distribution is significantly elongated in the direction of the lobes, as also visible in the images. There is less good agreement transverse to the lobe axis (Table 3) suggesting that the profile departs significantly from a β -model, especially at large radii where only the PSPC is sensitive. This is partly due to the faint excess emission to the north of the cluster visible in the PSPC image (Fig. 2). Given the better fit of the model to the HRI data, we prefer the parameters derived from this fit for the inner regions of the cluster. If we take the off-lobe HRI fit as representing the undisturbed cluster, we can interpret the on-lobe fit as suggesting that the lobes have pushed some material out of the core, extending the apparent core radius and steepening the profile at slightly larger radii.

We have seen that the X-ray emission is elongated along the radio axis. The maximum-resolution HRI image (Fig. 3) shows discrete structures superimposed on the radio lobes,

in particular arcs of emission perpendicular to the radio axis near the ends of each lobe. The brighter, western arc lies just beyond the brightest radio shell (or arc) embedded in the lobe. These features have been cited as evidence for a ‘radio/X-ray’ interaction by Siebert et al. (1999). The expected brightness from the smooth model of Table 2 at radii 74 and 88 arcsec (corresponding to the east and west X-ray arcs) is 2.2 ± 1.5 and 1.33 ± 1.3 HRI ct beam $^{-1}$, whereas the observed peaks are 5.7 and 6.8 ct beam $^{-1}$. (Because Poisson noise depends on the *expected* counts, errors are properly attached to the model rather than to the data). At low count levels, positive deviations are more probable than for a Gaussian noise distribution, so the eastern ‘arc’ is not very significant, but the western arc seems to be real. The other structures noted by Siebert et al. are only marginally significant, except for the most interesting, the ridge extending west from the core; unfortunately the latter is close enough to the core that it may be an artefact of pointing errors. As the discussion by Siebert et al. makes clear, there is no clear pattern in the relation between radio and X-ray features; e.g. the western jet is roughly superimposed on the X-ray ridge while the brighter eastern jet lies partly in an X-ray valley. Although Siebert et al. read the structure in terms of shells of material around the outer edges of the radio lobes, the enhanced emission is almost all seen projected *inside* the outer boundary of the radio lobes, which makes interpretation problematic. If these features are analogous to the enhancements around radio lobes seen in some other objects (e.g. Vir A, Belsole et al. 2001; Hyd A, Nulsen et al. 2002), then we would expect them to be cooler than the ambient ICM. Indeed, they are plausible candidates for the spectrally-detected ≈ 0.7 keV phase.

Notably lacking in the X-ray images are any clear depressions in the cluster gas associated with the radio lobes, of the kind found in Cyg A (Carilli et al. 1994; Wilson et al. 2000), Per A (Böhringer et al. 1993; Allen et al. 2001a), and several other DRAGNs (McNamara et al. 2000; Finoguenov & Jones 2001; Young et al. 2002). Given that the lobes of Her A are comparable in size to the cluster core, this is surprising, at least on the standard interpretation that the lobes are relativistic ‘bubbles’ which displace the thermal gas. Certainly, we cannot interpret the radio bridges as components of a cylindrically symmetric bubble passing straight through the cluster centre; this puzzle is discussed in detail in Paper II. Here we focus on the ‘bulbs’, that is, on the bright, roughly elliptical outer lobes. Fig. 9 shows the predicted X-ray brightness from our β -models for the Her A cluster, but with an ellipsoidal hole of zero X-ray emission matched in size to the radio bulbs. In Fig. 9a, the DRAGN is assumed to be in the plane of the sky. The brightness is reduced by a factor of almost two at the lobe centre. In Fig. 9b, we assume the DRAGN is inclined at 50° to the line of sight, as estimated in Paper III from our depolarization data. In Fig. 9c we take the cluster as elliptical, with the projected major and minor core radii as given by our sector fits. We assume the cluster is aligned with the radio lobes in three dimensions, i.e. both have 50° inclination. Finally, in Fig. 9d the cluster elongation is in the plane of the sky, but the radio source remains at $i = 50^\circ$. This gives very small distortions of the X-ray isophotes, although this geometry is contrived, implying as it does that the observed

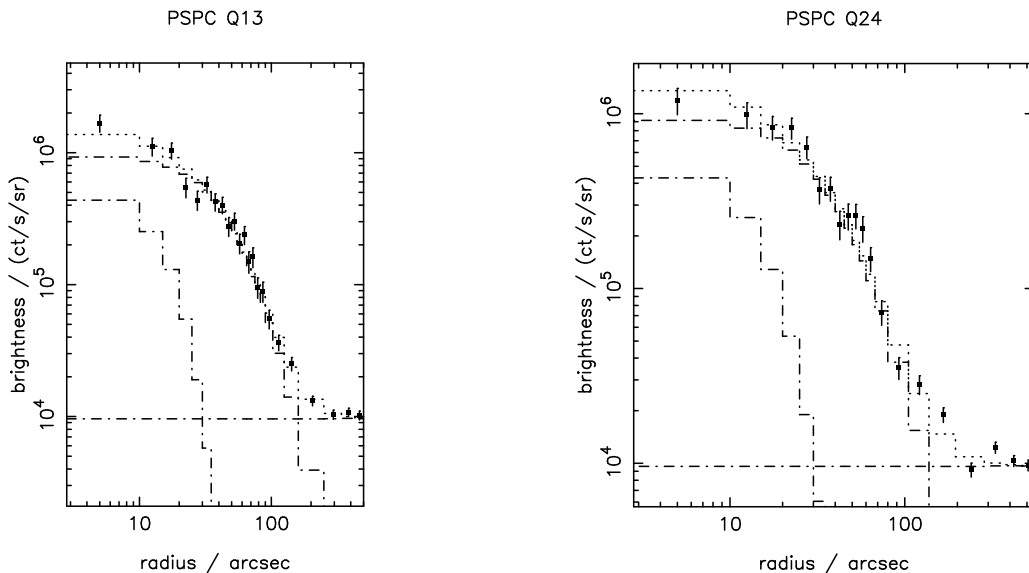


Figure 7. PSPC data: Radial profiles in sectors centered on- (left panel) and off- (right panel) the radio lobes.

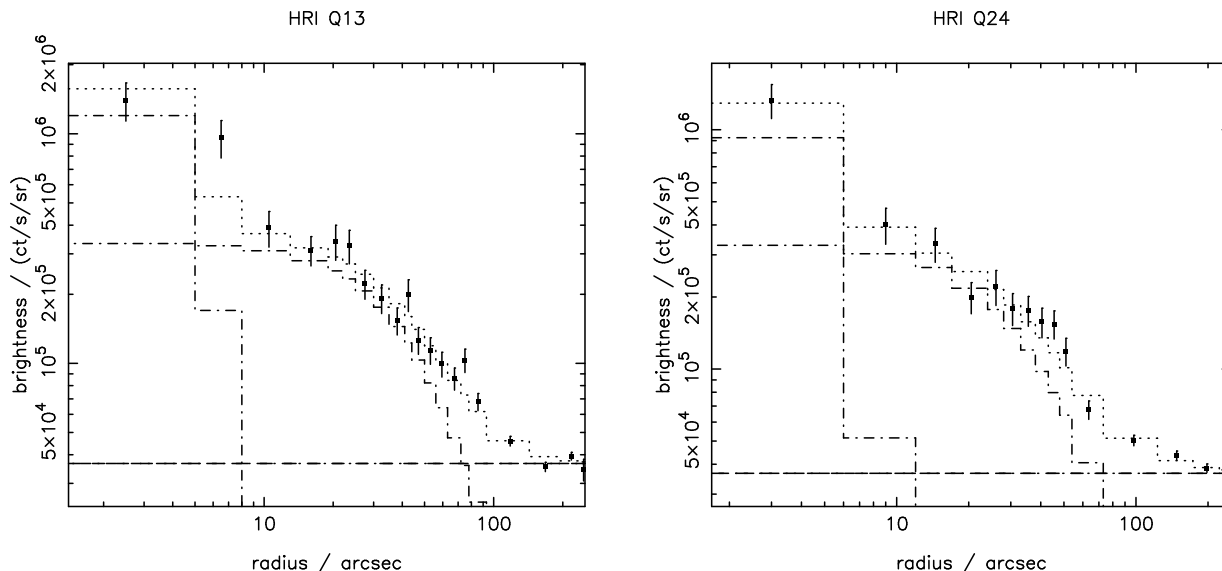


Figure 8. HRI data: Radial profiles in sectors centered on- (left panel) and off- (right panel) the radio lobes.

alignment between cluster and DRAGN is merely a chance projection effect.

The low signal-to-noise ratio in our HRI data, the low resolution of the PSPC, and the presence of the enhancements discussed above (which will partially mask any depressions), make it hard to exclude any of these models, although the case shown in Fig. 9a is certainly disfavoured. Our HRI image (Fig. 3) shows a ridge of emission along the northern edge of the western lobe, reminiscent of the generic features in Fig. 9 (but actually *more* prominent than in any of our models); but any ridges along the other lobe edges must be much weaker, at the level of the random fluctuations in the image. In short, our data are consistent with models in which the radio ‘bulbs’ are indeed empty of thermal gas, especially if we are correct in inferring that the radio axis is substantially out of the sky plane. Higher reso-

lutions and deeper observations with *Chandra* should clarify the details of this interaction (Wilson et al., 2003, in prep.).

5.2 Confinement of the radio lobes

As the radio lobes of Hercules A lack anything resembling hotspots, it seems likely that they are expanding at around the sound speed, and so are confined by the thermal pressure of the ambient ICM, rather than by strong shocks. Therefore a measurement of the thermal pressure should be a measurement of the energy density of the lobes. The lobes are sharply bounded (e.g. Fig. 5), suggesting little entrainment, so the lobe energy should be dominated by relativistic particles and fields. We therefore have the opportunity to test the minimum energy estimate u_{\min} with the more direct measurement from the external pressure.

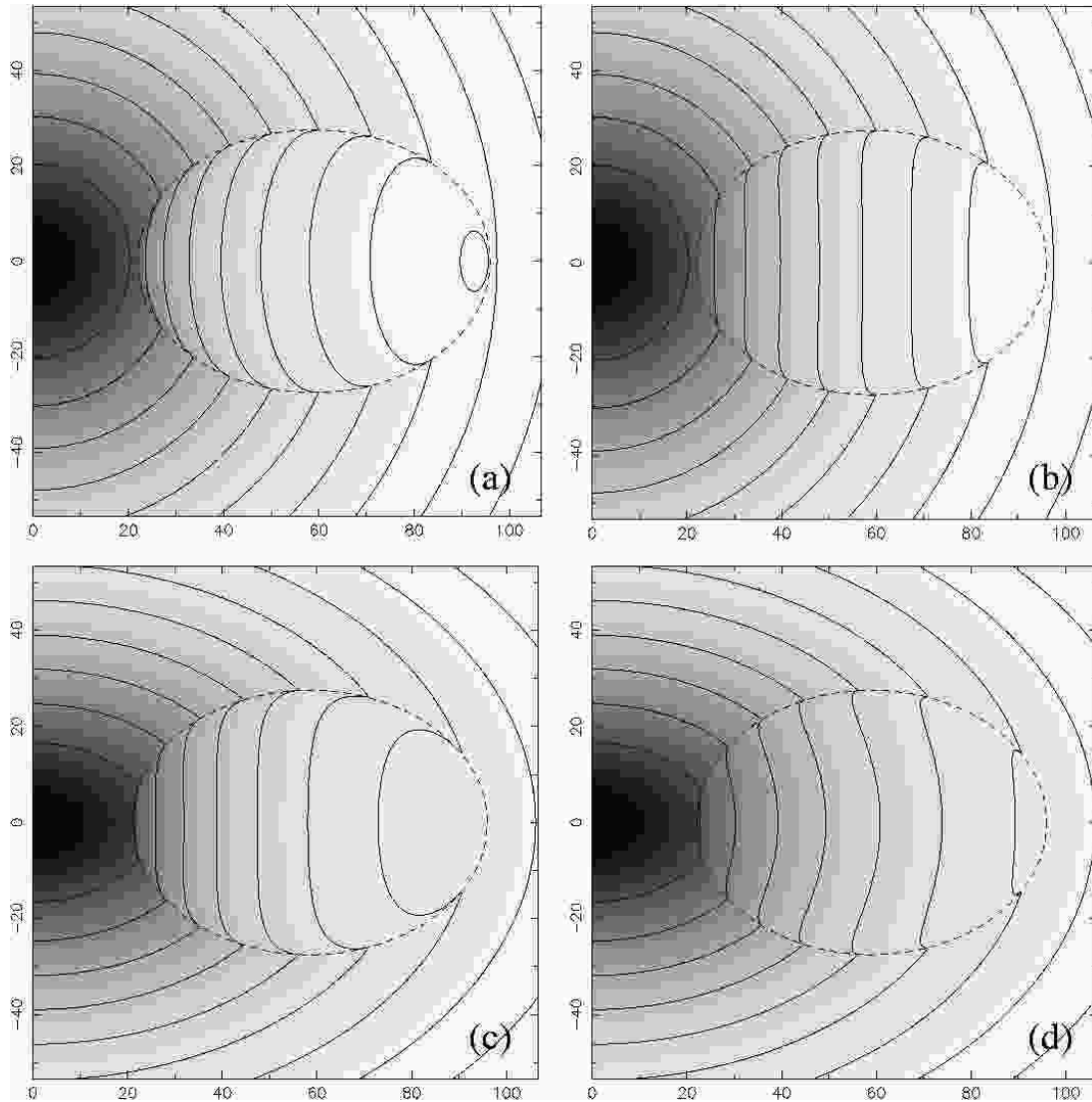


Figure 9. Models of the X-ray emission from β -model clusters with an ellipsoidal hole of zero emissivity, representing the radio lobe. In all cases the hole has major and minor projected axes 74 and 55 arcsec, its end is projected 96 arcsec from the cluster centre: the dashed ellipse shows its outline. The greyscale is linearly proportional to the model brightness, and the solid lines are X-ray isophotes separated by ratios of $\sqrt{2}$. We take $\beta = 0.74$ for all the cluster models. (a) Spherical cluster with $r_c = 43$ arcsec; radio axis inclination $i = 90^\circ$. (b) as in (a), but $i = 50^\circ$. (c) Elliptical cluster model with projected core radii 53 and 35 arcsec. Cluster and radio axis inclination both 50° . (d) as in (c) but cluster assumed to be in the plane of the sky, while the radio axis remains at $i = 50^\circ$.

As in Section 5.1, we focus on the bulbs rather than the faint inner lobes. Although the ends of the bulbs are at almost exactly the same distance from the centre, the more elliptical western bulb reaches closer to the middle and so on average is closer to the centre. Following the methodology of Leahy & Gizani (2001) we have calculated the minimum pressure ($P_{\min} = u_{\min}/3$) and the thermal pressure at the deprojected distance of the eastern and western bulbs of Hercules A, assuming $i \approx 50^\circ$. For the calculation of the thermal pressure, $P_{\text{th}} = 1.9n_e kT$, we have used the results of the combined fit of the surface brightness profile model (see Table 1). The results are listed in Table 4: R is the deprojected distance of the bulb centres, while B_{me} is the

Table 4. Minimum energy parameters and the thermal pressure

Component	R arcsec	B_{me} nT	P_{\min} pPa	P_{th} pPa	B_{MS} nT	P_{MS} pPa
East bulb	84	0.79	0.19	2.3	1.99	1.05
West bulb	71	0.73	0.17	3.0	1.86	0.92

minimum energy magnetic field. In addition to the conventional minimum energy parameters we also list the values B_{MS} and P_{MS} found using the methodology presented in Myers & Spangler (1985), that is, assuming the electron energy spectrum extends down to a Lorentz factor of 10.

As we can see from Table 4, the radio lobes of Hercules A would be significantly underpressured with the standard minimum energy assumptions for the radio plasma: electron/positron composition (i.e. no protons), filling factor unity and a low-energy cutoff corresponding to 10 MHz emission. Thus minimum energy is a severe underestimate of the actual energy content of the lobes, by an order of magnitude.

Such a deficit in the minimum energy has been established for a long time for FRI DRAGNs (e.g. Feretti, Perola & Fanti 1992), but FRI jets and tails were often modelled as turbulent flows with substantial entrainment, so the result could be attributed to mixture with the ambient gas and/or to a low filling factor for the radio plasma. This was ruled out in some FRIs by the discovery of X-ray cavities (Böhringer et al. 1993; McNamara et al. 2000), and by deficits in cases like Her A, where the lobes are sharply bounded (Hardcastle & Worrall 2000a; Leahy & Gizani 2002). This points to an error in the microphysical assumptions, as discussed in detail by Leahy & Gizani (2001) for 3C 388. In that case we argued that the extra energy is mostly in the form of particles, and as a result the magnetic field should be below equipartition and therefore does not play an important role in the lobe dynamics. The results of the Myers & Spangler calculations show that an alternative option is available for Her A: equipartition can be (almost) preserved if the particle energy spectrum extends down to trans-relativistic energies. The difference arises essentially because the steeper spectrum of Her A gives a larger increase in energy on extrapolating to low Lorentz factors.

5.3 Cooling and heating of the cluster gas

The intracluster gas is densest in the core of the cluster and therefore the radiative cooling time t_{cool} , due to the emission of the observed X-rays is shortest there (Fabian, Nulsen & Canizares 1991; Fabian 1994). For isobarically cooling gas

$$t_{\text{cool}} = \frac{\frac{5}{2}kT(n_H + n_e + n_{He})}{\Lambda(T, Z)n_e n_H} = \frac{5.75 kT}{\Lambda(T, Z) n_e} \quad (3)$$

$$\approx 10^{11} \left(\frac{n_e}{10^3 \text{ m}^{-3}} \right)^{-1} \left(\frac{T}{10^8 \text{ K}} \right)^{\frac{1}{2}} \text{ yr}$$

where $\Lambda(T, Z)$ is the cooling function (see Leahy & Gizani 2001). The last form is the approximation of Sarazin (1986), which begins to become inaccurate for temperatures below 3 keV. For the centre of the Hercules A cluster the cooling time is 6.4 Gyr if the hot phase dominates, but ≈ 2 Gyr if the core is dominated by the cool phase. Since this is less than the age of the universe, this would normally imply the presence of a cooling flow (Sarazin 1986). The cooling radius, i.e. the radius at which the cooling time equals 10^{10} yr, is ≈ 90 kpc, somewhat less than the core radius, consistent with the relatively good fit to the β model.

Peres et al. (1998) find that the core radii of cooling flows clusters is generally smaller than in non-cooling flow clusters, with the division around 130 kpc, which also suggests that Her A has a cooling flow. However, the Peres et al. core radii are fitted values for the (assumed isothermal)

cluster *mass* distribution, and are not directly comparable to *gas* core radii derived from β -model fits.

It now appears that in many or all clusters, some agency prevents fully formed cooling flows from developing, so that little gas cools to much less than half the ambient cluster temperature (see Molendi & Pizzolato 2001; Peterson et al. 2003 for recent analyses). Energy input from DRAGNs is a popular candidate for this agency, (e.g. Churazov et al. 2002, and references therein). Attention has mostly been focussed on weaker, quasi-continuous AGN activity rather than major episodic outbursts as in Her A, but the latter may also play an important rôle (e.g. David et al. 2001).

Although our results show that the normal state of the Hercules A cluster is a cooling flow, a region a few times the size of the core is now affected by the expansion of the radio lobes, and it is easy to see that the ‘waste’ energy supplied to the environment by the DRAGN currently far outweighs the energy loss from X-ray radiation. If we assume quasi-isobaric (and so subsonic) expansion, so that the cluster pressure distribution is not disturbed, the average rate of work done by the DRAGN is $dW/dt = \int_{\text{lobes}} p dV/\tau$ where τ is the lifetime. As in Section 5.1 we focus on the outer ‘bulbs’ of the lobes, and we model these as prolate ellipsoids inclined at $i \approx 50^\circ$; numerical integration gives a ‘pressure content’ of $\sim 5 \times 10^{53}$ J. Writing $\tau = \tau_8 \times 10^8$ yr, this gives $dW/dt \sim 1.6\tau_8^{-1} \times 10^{38}$ W. The combined kinetic power of the jets $K = 4 dW/dt$, as it equals the enthalpy flux into the lobes (we assume that the lobes are dominated by relativistic plasma, so $u = 3P$). We can also parameterize the problem in terms of the radiative efficiency of the DRAGN. With the radio luminosity $L_{\text{radio}} = 3.8 \times 10^{37}$ W,

$$\varepsilon = L_{\text{radio}}/K \approx 0.06\tau_8,$$

and we can write $dW/dt = L_{\text{radio}}/4\varepsilon$. Estimates for the lifetimes of powerful DRAGNs are typically in the range $0.1 \lesssim \tau_8 \lesssim 1$, corresponding to an efficiency of 0.6–6 per cent for Her A. Given that the radio luminosity of the DRAGN and the X-ray luminosity of the entire cluster are almost the same, the cluster gas is currently gaining energy at 3–30 times its radiative loss rate. Reynolds, Heinz & Begelman (2001) point out that initially the work done may appear as potential energy (some of the gas is lifted out of the cluster core); in the long term much of this will be re-cycled to heat via turbulent dissipation. In supersonic expansion, of course, there will be at least some direct heating by shocks. In either case, any cooling of the cluster will be temporarily reversed. When the radio outburst is over, the cluster will return to its cooling state. At present, most of the mechanical energy is being deposited well outside the cluster core, and it is possible that the core is already cooling again, even while the outer part of the cluster is heated.

If the efficiency is around 1 per cent, and the AGN is periodically active with a duty cycle of around 4 per cent, then on average radiative cooling of the cluster is balanced by mechanical heating. The cooling time of the cluster would then provide a rough measure of the time since the last outburst. Such a scenario appears to suffer from fine tuning (Fabian et al. 2001), but, as suggested by Churazov et al. (2002), feedback via accretion onto the AGN from the cooling gas could naturally regulate the cycle of heating and cooling.

Although it is most likely that Her A is expanding tran-

sonically, it is interesting to consider how compression of the cluster gas behind the bow shock of a DRAGN will affect the cooling time. We have found how the Mach number changes the cooling time, by using the Sarazin (1986) approximation, and the change in temperature and density as a function of shock Mach number (Landau & Lifshitz 1959). For shock normal Mach numbers $\mathcal{M} < 6.5$ the cooling time is initially somewhat reduced, but only by up to around 40 per cent, which is not nearly enough to make radiative losses important on the timescale of the AGN ($\lesssim 10^8$ yr). Over the longer term, the material will re-expand adiabatically to a condition with a longer cooling time than before. Higher Mach numbers will increase the cooling time from the start, but for $\mathcal{M} \gtrsim 10$ the shocked gas will be too hot to be visible in X-rays. We note that in the case of Hercules A the pre-shock central cooling time would have been $< 10^{10}$ yr whatever the Mach number, i.e. the apparent cooling flow cannot be an artefact of the DRAGN.

5.4 The magnetic field in the cluster core

In Paper III we estimate the strength of the intracluster magnetic field as a function of radius, using our X-ray data and the Faraday dispersion from our radio data. In this section we attempt a cruder estimate, using the dispersion of the rotation measure σ_{RM} in the central $r_c = 43.4$ arcsec. We follow the analysis by Garrington & Conway (1991), who show that the expected σ_{RM} for a source behind a Faraday screen with a tangled magnetic field with rms B nT (independent of radius), is given by

$$\sigma_{RM} = 0.0081 \left[\int (n_e B_{\parallel})^2 l dz \right]^{1/2} \quad (4)$$

where z is along the line of sight, l is the coherence length, (both in kpc), n_e is electron density in m^{-3} , and B_{\parallel} is the component of the field parallel to z , equal to $B/\sqrt{3}$ for isotropic tangling. For a source at the center of a cluster whose radial profile is described by a β -model this becomes (e.g. Felten 1996)

$$\sigma_{RM} = \frac{0.0081 B_{\parallel} n_0 r_c^{1/2} l^{1/2}}{(1 + r^2/r_c^2)^{(6\beta-1)/4}} \sqrt{\frac{\pi^{1/2} \Gamma(3\beta - 0.5)}{2\Gamma(3\beta)}}, \quad (5)$$

where n_0 is the central electron density and Γ is the Gamma function. Figure 10 is a histogram of the rotation measure for all significant pixels in Her A within the core radius, from our radio data (Paper III). We find $\sigma_{RM} = 214$ rad m^{-2} , and the coherence length l near the centre is about 5 arcsec or 14 kpc (Paper III). We take a fiducial value of $r = 80$ kpc (28.6 arcsec), since most of the pixels with valid rotation measures are towards the outer part of the region. Then, using n_0 , β and r_c from our combined HRI and PSPC fit, the estimated $B \simeq 0.2$ nT. Hence the magnetic field in the central region of the cluster of Hercules A is lower than in extreme cooling flow clusters (e.g. the 3C 295 cluster, Allen et al. 2001b), but within the typical range for clusters in general (Carilli & Taylor 2002).

5.5 The central source

As we have seen in Section 4 the improvement of fitting a blurred PSF to the central peak is insignificant. This means

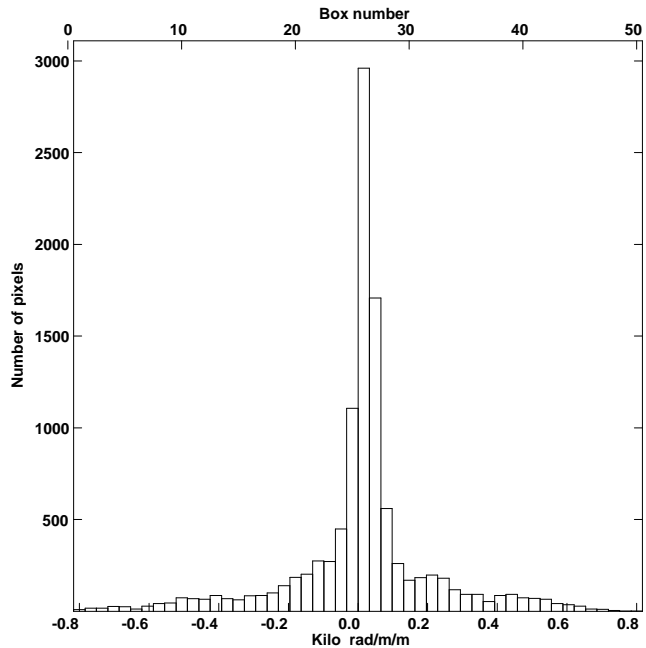


Figure 10. Histogram of the rotation measure for all significant pixels within 43.4 arcsec of the radio core of Her A, from our radio data (Paper III).

that both a nominal PSF and a blurred PSF are both good fits of the weak central peak in the HRI image (for example see Fig. 3). All we can say is that we have a central source with a count rate of 0.009 ct s^{-1} in our hard band (Table 1). The peak could be either an AGN or a galaxy-scale cooling flow. We will discuss each case separately:

5.5.1 The central source as an AGN

We have already noted that there is no sign of an obscured AGN in the high-energy *BeppoSAX* spectrum (Trussoni et al. 2001), so we assume a power-law model with only Galactic absorption. Assuming a typical photon index of $\Gamma = 1.9$, the unabsorbed 0.1–2.4 keV luminosity of the central source is then 2.0×10^{36} W. At 5 GHz, the radio core luminosity is 7.1×10^{23} W Hz^{-1} . The point source appears a few times over-luminous in X-rays relative to the correlation between L_X and radio core power for galaxies (Siebert et al. 1996, corrected to our H_0), although it lies within the general scatter. We note that Siebert et al’s correlation is formed mostly by broad-line objects, while Her A is a low excitation radio galaxy (Tadhunter et al. 1993; Jackson & Rawlings 1997), with a steep spectrum (optically thin) radio core at GHz frequencies (Paper II). Although X-ray variability is expected in an AGN we have not detected any during the interval of the two and a half years between our PSPC and HRI observations. AGN X-ray emission could be synchrotron or inverse Compton. Hardcastle & Worrall (2000b) have argued that inverse Compton is required, at least in FR Is, if the unified model of low-power radio galaxies and BL Lacs is correct.

5.5.2 The central source as a cooling flow

The extra broadening by the PSF that fits the data best corresponds to the nominal PSF convolved with a gaussian of FWHM 5.0 arcsec. Therefore the width of the cooling flow peak, if any, would have to be around 5.0 arcsec or less. In contrast the cluster core radius found from the fits is 43 arcsec, an order of magnitude larger. This would give the cluster emission a ‘prussian hat’ look: essentially the central peak is on the scale of the central cD galaxy rather than the cluster. Small central peaks like this are sometimes seen in cooling flows. The X-ray luminosity is just greater than the largest value for an individual galaxy in the *Einstein Observatory* sample of Eskridge, Fabbiano & Kim (1995), but this sample excluded cluster-centre galaxies. This suggests that if the central source is thermal emission it relates to the cluster and/or the AGN, rather than solely to the host galaxy. In this case the central source, at around 5 per cent of the cluster luminosity, would presumably contribute to the cool component detected in the spectrum, but could not produce all of it, as previously noted.

6 CONCLUSIONS

Our *ROSAT* PSPC and HRI X-ray observations of the intracluster gas in the Hercules A cluster have revealed an extended X-ray emission, extending to radius 2.2 Mpc (PSPC data) and a weak central peak (HRI data).

Based on discrepancies between single-temperature fits to the PSPC, *ASCA* and *BeppoSAX* spectra, we argue that the intracluster gas contains at least two phases, dominated by a ≈ 4 keV component (seen by *ASCA* and *BeppoSAX*), but with around 15 per cent of the emission in the *ROSAT* band from material at 0.5–1 keV. This model significantly improves the PSPC fit compared to one with a single temperature. The 0.1–2.4 keV (absorbed) flux density is 3.0×10^{-15} W m $^{-2}$, and the bolometric luminosity is 4.8×10^{37} W. There is no evidence for absorption above the Galactic value.

We have detected X-ray emission coming from a compact source at the centre of the cluster, with a 0.1–2.4 keV luminosity of 2×10^{36} W. Our data does not distinguish between an AGN and galaxy-scale thermal emission (perhaps a central cooling-flow spike). The central electron density (excluding the central source) is $n_0 \approx 1.0 \times 10^4$ m $^{-3}$. The central cooling time is in the range 2–6 Gyr, depending on whether or not the cool gas phase is concentrated in the centre. The cooling radius is 90 kpc. The cluster core should therefore be a cooling flow if we ignore the effect of the DRAGN. Indeed, most of the time, the DRAGN will be absent, as its life-time is certainly short compared to the age of the Universe. But at present the DRAGN, which is several times larger than the cooling radius, is almost certainly depositing more energy into this region of the ICM than is being lost radiatively.

Our best combined (PSPC and HRI) fit to the surface brightness profile, with a model consisting of a PSF, a β model and a background, gives a β parameter of 0.74 ± 0.03 , typical for clusters of galaxies. The radio lobes are largely positioned beyond the X-ray core radius, allowing for projection, so they are expanding essentially into a power-law atmosphere with density falling as $r^{-3\beta} \sim r^{-2.22}$, quite

close to the r^{-2} profile needed to give the lobes a self-similar structure (Falle 1991).

The thermal pressure at the deprojected distance of the radio lobes is an order of magnitude larger than the minimum pressure of the lobes. Thus the minimum energy in the lobes is a severe underestimate of the actual energy content. This seems to be typical for DRAGNs, of both FR types, although only in a few cases can it be established as clearly as in Her A.

Two features of the X-ray emission may result from the interaction of the cluster gas with the radio lobes. The region around the core of the cluster is clearly elongated along the radio axis, as revealed by our on- and off-lobe profiles. In addition there are a number of apparently discrete X-ray enhancements projected on or around the radio lobes; however some of these may be artefacts or due to poor photon statistics in our ROSAT data. Unlike some other well-studied DRAGNs, Her A as yet does not show X-ray holes coincident with the radio lobes. But we have shown that the such holes could be too shallow to detect in our data, due to projection effects: the main lobes being displaced along the line of sight away from the X-ray bright region around the cluster core. Deep observations with *Chandra* should reveal some sign of these holes, if present, and also clarify the nature of the ‘enhancements’.

ACKNOWLEDGMENTS

We thank Megan Donahue for helpful discussions.

Nectaria Gizani would like to acknowledge: PPARC for funding her fees for three years to carry out her PhD work at Jodrell Bank at the University of Manchester; The grant PRAXIS XXI/BPD/18860/98 from the Fundação para a Ciência e a Tecnologia, Portugal for the post-doctoral fellowship; The current post-doctoral grant under contract 332 from the State Scholarships Foundation (IKY), Greece. NG is grateful to Jodrell Bank Observatory for the support of a post-doctoral fellowship.

This research has made use of the NASA/IPAC Extragalactic Database (NED) which is operated by the Jet Propulsion Laboratory, Caltech, under contract with the national aeronautics and space administration. It has also made use of NASA’s Astrophysics Data System Abstract Service (ADS).

We thank the UK ROSAT Data Archive Centre at the Department of Physics and Astronomy, Leicester University and the ROSAT group. We used the XSPEC and ASTERIX software packages, and thank their creators and maintainers.

REFERENCES

- Abell G. O., 1958, ApJS, 3, 211
- Allen S. W., Fabian A. C., 1998, MNRAS, 297, L57
- Allen S. W., Fabian A. C., Johnstone R. M., Arnaud K. A., Nulsen P. E. J., 2001a, MNRAS, 322, 589
- Allen S. W. et al., 2001b, MNRAS, 324, 842
- Anders E., Grevesse N., 1989, Geoch. et Cosmoch. Acta, 53, 197
- Balucinska-Church M., McCammon D., 1992, ApJ, 400, 699

- Barthel P. D., Arnaud K. A., 1996, MNRAS, 283, L45
 Baum S. A., O'Dea C. P., De Koff S., Sparks W., Hayes J. J. E., Livio M., Golombek D., 1996, ApJ, 465, L5
 Belsole E. et al., 2001, A&A, 365, L181
 Bertschinger E., Meiksin A., 1986, ApJ, 306, L1
 Böhringer H., Voges W., Fabian A. C., Edge A. C., Neumann D. M., 1993, MNRAS, 264, L25
 Briel U. G. et al., 1996, ROSAT User's Handbook. Max-Planck-Institut für Extraterrestrische Physik, p. 34
 Carilli C. L., Perley R. A., Harris D. E., 1994, MNRAS, 270, 173
 Carilli C. L., Taylor G. B., 2002, ARAA, 40, 319
 Cavaliere A., Fusco-Femiano R., 1978, A&A, 70, 677
 Churazov, E., Sunyaev, R., Forman, W., Böhringer, H., 2002, MNRAS, 332, 729
 Cirimele G., Nesci R., Trèvese D., 1997, ApJ, 475, 11
 Colgan S. W. J., Salpeter E. E., Terzian Y., 1988, ApJ, 328, 275
 David L. P., Harnden F. R., Kearns K. E., Zombek M. V., 1998, www.harvard.edu/rosat/rsdc/www/hricalrep.html
 David L. P., Nulsen, P. E. J., McNamara, B. R., Forman, W., Jones, C., Ponman, T., Robertson, B., Wise, M., 2001, ApJ, 557, 546
 Dreher J. W., Feigelson E. D., 1984, Nat, 308, 43
 Ebeling H., Edge A. C., Böhringer H., Allen S. W., Crawford C. S., Fabian A. C., Voges W., Huchra J. P., 1998, MNRAS, 301, 881
 Eskridge P. B., Fabbiano G., Kim D., 1995, ApJS, 97, 141
 Fabian A. C., 1994, ARAA, 32, 277
 Fabian A. C., Mushotzky R. F., Nulsen P. E. J., Peterson J. R., 2001, MNRAS, 321, L20
 Fabian A. C., Nulsen P. E. J., Canizares C. R., 1991, A&AR, 2, 191
 Falle S. A. E. G., 1991, MNRAS, 250, 581
 Feigelson E. D., Berg C. J., 1983, ApJ, 269, 400
 Felten, J. E., 1996, in Trimble, V. & Reisenegger, A. (eds), Clusters, Lensing, and the Future of the Universe, ASP Conf. Ser. 88, p. 271
 Feretti, L., Perola, G. C., Fanti, R., 1992, A&A, 265, 9
 Finoguenov A., Jones C., 2001, ApJ, 547, L107
 Garrington, S. T., Conway, R. G., 1991, MNRAS, 250, 198
 Gizani N. A. B., Leahy J. P., 1996, in Ekers R. D., Fanti C., Padrielli L., eds, Extragalactic Radio Sources, IAU Symp. 175, Kluwer, p. 351
 Gizani N. A. B., Leahy J. P., 1999, New. Astr. Rev., 43, 639
 Gizani N. A. B., Leahy J. P., 2003, MNRAS, 342, 399 (Paper II)
 Greiner, J., Tovmassian, G. H., DiStefano, R., Prestwich, A., González-Riestra, R., Szentasko, L. & C. Chavarría, C., 1999, A&A, 343, 183.
 Hardcastle, M. J., Worrall, D. M. & Birkinshaw, M., 1998, MNRAS, 296, 1098
 Hardcastle M. J., Worrall D. M., 2000a, MNRAS, 309, 969
 Hardcastle M. J., Worrall D. M., 2000b, MNRAS, 314, 359
 Hasinger G., Turner T. J., George I. M., Boese G., 1995, OGIP Calibration Memo CAL/ROS/92-001
 Jackson N., Rawlings S., 1997, MNRAS, 286, 241
 Jones C., Forman W., 1984, ApJ, 276, 38
 Kaastra J. S., 1992, Technical report, An X-ray Spectral Code for Optically Thin Plasmas. Internal SRON-Leiden Report, updated version 2.0
 King I., 1962, AJ, 67, 471
 Landau L. D., Lifshitz E. M., 1959, Fluid Mechanics, Pergamon Press, Oxford
 Leahy J. P., 1993, in Röser, H. J., Meisenheimer, K., eds, *Jets in Extragalactic Radio Sources*, Springer-Verlag, Berlin, p. 1
 Leahy J. P., Gizani N. A. B., 2001, ApJ, 555, 709
 Leahy J. P., Gizani N. A. B., 2002, New. Astr. Rev., 46, 117
 Ledlow M. J., Owen F. N., 1996, AJ, 112, 9
 McNamara B. et al., 2000, ApJ, 534, L135
 Molendi S., Pizzolato F., 2001, ApJ, 560, 194
 Myers S. T., Spangler S. R., 1985, ApJ, 291, 52
 Nulsen P. E. J., David L. P., McNamara B. R., Jones C., Forman W. R., Wise M., 2002, ApJ, 568, 163
 Osborne J., 1993, Rosat UK Newsletter, No. 6, 8
 Owen F. N., Laing R. A., 1989, MNRAS, 238, 357
 Peres C. B., Fabian A. C., Edge A. C., Allen S. W., Johnstone R. M., White D. A., 1998, MNRAS, 298, 416
 Peterson J. R., Kahn S. M., Paerels F. B. S., Kaastra J. S., Tamura T., Bleeker J. A. M., Ferrigno C., Jernigan J. G., 2003, ApJ, submitted, astro-ph/0210662
 Reynolds C. S., Heinz S., Begelman M. C., 2001, ApJ, 549, L179
 Sadun A. C., Hayes J. J. E., 1993, PASP, 105, 379
 Sarazin G. L., 1986, Phys. Rev., 58, 1
 Scharf C. A., Mushotzky R. F., 1997, ApJ, 485, L65
 Siebert J., Brinkmann W., Morganti R., Tadhunter C. N., Danziger I. J., Fosbury R. A. E., Di Serego Alighieri S., 1996, MNRAS, 279, 1331
 Siebert J., Kawai N., Brinkmann W., 1999, A&A, 350, 25
 Stark A. A., Gammie C. F., Wilson R. W., Bally J., Linke R. A., Heiles C., Hurwitz M., 1992, ApJS, 79, 77
 Tadhunter C. N., Morganti R., Alighieri S. S., Fosbury R. A. E., Danziger I. J., 1993, MNRAS, 263, 999
 Trussoni E., Feretti L., Massaglia S., Parma P., 2001, A&A, 366, 788
 White D. A., Jones C., Forman W., 1997, MNRAS, 292, 419
 Wilson A. S., Young A. J., Shopbell P. L., 2000, ApJ, 544, L27
 Yates M. G., Miller L., Peacock J. A., 1989, MNRAS, 240, 129
 Young A. J., Wilson A. S., Mundell C. G., 2002, ApJ, 579, 560